ELSEVIER

International Journal of Heat and Fluid Flow 22 (2001) 393–401

International Journal of HEAT AND FLUID FLOW

www.elsevier.com/locate/ijhff

Turbulence statistics of periodically perturbed separated flow over backward-facing step

Shuya Yoshioka, Shinnosuke Obi, Shigeaki Masuda *

Department of Mechanical Engineering, Keio University, 3-14-1 Hiyoshi, Kohoku-ku, Yokohama 223-8522, Japan

Received 14 July 2000; accepted 26 January 2001

Abstract

The turbulence statistics of an unsteady separated flow was experimentally investigated. A backward-facing step flow at $Re = 3700$ was chosen as the test case, where periodic perturbation was introduced from its step edge. A two-dimensional particle imaging velocimeter (PIV) was used in the flow-field measurement. The measured results showed that the reattachment length was reduced by the applied periodic perturbation. There existed an optimum frequency for the promotion of the reattachment. When perturbed at the optimum frequency, $St = 0.19$, the reattachment length was reduced by 30%. The Reynolds stress components were increased by the perturbation, and their distribution varied with the perturbation frequency. When perturbation at the optimum frequency was applied, Reynolds stress markedly increased near the reattachment zone. This increase in Reynolds stress enhanced the momentum transfer across the shear layer, enabling the promotion of the reattachment. On the other hand, the region where the perturbation at higher frequency than the optimum frequency increases Reynolds stress was limited immediately behind the step. The perturbation at lower frequency than the optimum frequency increased Reynolds stress in the region downstream of the reattachment zone. Therefore, both low- and high-frequency perturbations have less effect on the promotion of the reattachment than optimum-frequency perturbation.

Keywords: Flow control; Separation; Shear flow; Backward-facing step; Turbulent flow; Unsteady flow; PIV

1. Introduction

The performance of fluid machinery is greatly influenced by the occurrence of the flow separation and reattachment phenomena. The control of separated flow has been one of the important goals of fluids engineering. To control the reattachment of the separated flow, continuous suction or injection to the shear layer has been applied to various types of flow configurations. Recent studies showed that alternating suction and injection, namely, periodic perturbation, exhibited better reattachment control than continuous perturbation (Nishri and Wygnanski, 1998; Seifert and Pack, 1999). A detailed investigation of the control of turbulent separated flow by periodic perturbation is desired.

There has been much research interest on the periodically perturbed turbulent separated flow. The first interest is related to the active control of the reattachment process, in which the enhancement of momentum transport across the separated shear layer plays a major role (Sigurdson, 1995; Chun and Sung, 1996). The second and rather fundamental interest is the excitation of the inflectional instability and vortex formation inherent to the separated shear layer as well as the spectral transport of energy from a given perturbation frequency to the other frequency range (Bhattacharjee et al., 1986; Kiya et al., 1997; Chun and Sung, 1998). This kind of investigation may contribute to the understanding of the fundamental mechanism of unsteady separated flows. The third one is the effect of external forcing on the distributions of turbulence quantities. Their accurate measurement would be useful for the evaluation of the schema for numerical prediction of unsteady separated flows. This may attract the attention of those who are interested in the extension of the turbulence model to unsteady separated flow problems. For this purpose, highly accurate and sophisticated data sets are desired, covering higher order turbulence statistics (Masuda et al., 1994). Although all these interests cannot be discussed separately, the investigations reported so far have been mainly limited to the motion of vortical structures in the separated shear layer.

One of the early attempts of flow control by periodic perturbation was made by Bhattacharjee et al. (1986). They applied acoustic perturbation to a flow behind a backward-facing step, and revealed that the enhancement of the spread of the shear layer occurred due to the production of large-scale vortical structures in the shear layer, enabling the promotion of reattachment. Chun and Sung (1996) discovered that large-

* Corresponding author. Tel.: +81-45-566-1517; fax: +81-45-566-1517.

E-mail address: smasuda@mech.keio.ac.jp (S. Masuda).

0142-727X/01/$ - see front matter
PII: S0142-727X(01)00079-0

Notation

f_e	perturbation frequency
H	step height
P_{ij}	production rate of Reynolds stress
Re	Reynolds number, $Re = U_c H/v$
S	standard deviation
St	Strouhal number, $St = f_e H/U_c$
U_c	center velocity of the inlet channel
$\hat{u}_i$	instantaneous velocity, $\hat{u}_i = U_i + \tilde{u}_i + u'_i$
U_i	mean velocity component
$\tilde{u}_i$	periodic component of velocity
u'_i	turbulent component of velocity
u_i	total fluctuation component of velocity, $u_i = \tilde{u}_i + u'_i$
$\overline{u_i u_j}$	Reynolds stress
u_τ	friction velocity
v_e	injection velocity at the slit exit
V_e	perturbation amplitude
x, y, z	streamwise, normal and spanwise coordinates
x_R	reattachment length

Greek symbol

v	kinetic viscosity

Subscripts

b	bulk mean value
c	center value at inlet channel
rms	root-mean-square value
0	value without perturbation

Superscripts

+	normalized by wall variables
¯	time average

scale vortices which were introduced into the shear layer by periodic perturbation merged with each other in the separated shear layer, enabling shear layer development. Sigurdson (1995) applied periodic perturbation to a shear flow downstream of a sharp-edged blunt face of a circular cylinder aligned coaxially with the free stream, and revealed that the reattachment was enhanced by perturbation at a frequency that nearly corresponded to the natural vortex-shedding frequency. The main conclusions of the above studies were the existence of an optimum frequency range for reattachment promotion and the promotion of the vortex merging process by perturbation over the optimum-frequency range.

The main objective of this study is to clarify the mechanism of the enhancement of momentum transfer by the applied perturbation. The second objective is to investigate the perturbation-frequency characteristic of this effect of momentum transfer enhancement and the third one is to explain the existence of an optimum frequency for perturbation for reattachment promotion. The experiment is conducted in a two-dimensional turbulent separated flow over a backward-facing step, where perturbation is applied as an alternating suction and injection from its step edge. For flow-field measurement, a two-dimensional particle imaging velocimeter (PIV) is employed to capture the flow structure that is widely distributed in the separated shear layer.

2. Experimental apparatus

2.1. Water channel facility

The experiments were performed in a closed loop facility using water as shown in Fig. 1. Flow was driven by centrifugal pump 2 (0.75 kW) and passed through settling chamber 4, contract section 5 (contraction ratio is 0.12), and honeycomb 6 before entering test section 9. In settling chamber 4, two screens were installed in tandem to maintain water flow. At the upstream of the test section, the water passed through rectangular channel 8 of 40 mm high, 240 mm wide and 1020 mm long. In this channel, two tripping wires (3 mm in diameter) 7 were put on each wall. Honeycomb 10 was set at downstream of the test section to avoid a corner effect.

2.2. Test section

The test section, shown in Fig. 2(a), was made of acrylic resin to enable flow visualization. The step height H was

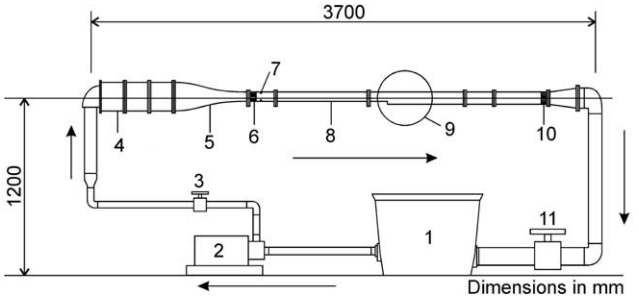

Fig. 1. Water channel facility; 1 – tank, 2 – pumb, 3 – valve, 4 – setting chamber, 5 – contract section, 6 – honeycomb, 7 – tripping wire, 8 – entrance region, 9 – test section, 10 – honeycomb, 11 – valve.

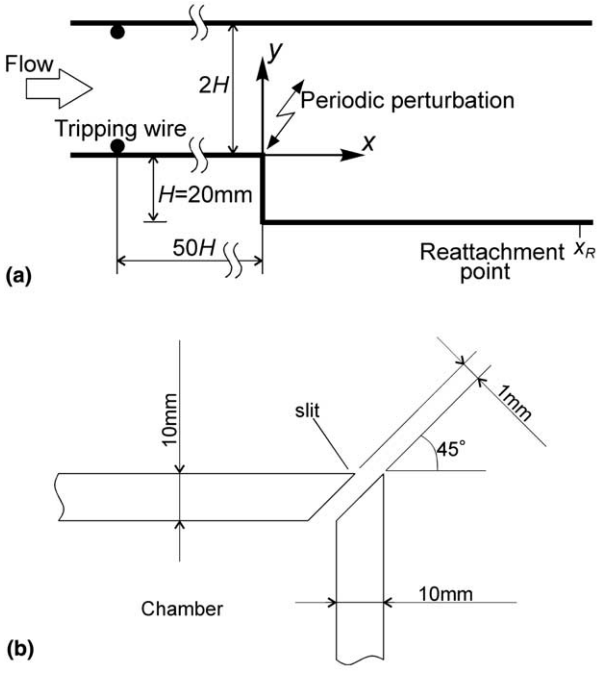

Fig. 2. Schematic of the test section: (a) test section; (b) details of step edge.

20 mm, resulting in expansion ratio of 2:3. The aspect ratio based on H and channel span was 1:12. As illustrated in Fig. 2(a), the origin of the Cartesian coordinate system was fixed at the center of the step edge. The x-axis was directed downstream and the y-axis was directed to the opposite side wall. The spanwise uniformity of the flow was confirmed in the region $-3.0 < z/H < 3.0$ by the preliminary experiment. A spanwise slit, 1 mm in width, was opened at the step edge, as shown in Fig. 2(b). Periodic perturbation was introduced through this slit as an alternating suction and injection in the direction 45° relative to the x-axis.

The perturbation was generated by driving a piston of a syringe that was moved by a digitally controlled electric motor and introduced to the chamber inside of the step through a rigid silicon tube. Therefore, as far as the incompressible fluid was used, the syringe piston movement directly corresponds to the fluid motion at the outlet of the slit. The perturbation was designed to follow the expression:

$$v_e = V_e \sin(2\pi f_e t), \tag{1}$$

where v_e was the injection velocity at the slit exit with V_e being the amplitude and f_e the frequency of the perturbation. V_e was set constant to 30% of U_c throughout the experiment. According to the previous experiments, the effect of perturbation increased linearly to the amplitude upto 30% of U_c, and saturated above it. The experiments were undertaken at the condition where the most pronounced effects were exhibit.

3. Velocity measurement

3.1. Flow visualization and image acquisition

An in-house-made two-dimensional PIV was employed for flow-field measurement. Nylon12 particles, 90 μm in mean diameter and 1.02 in specific gravity, were seeded uniformly in the water flow as the tracer. Two independent Xenon stroboscopes were used as the light source in PIV measurement. The light was led through an optical fiber from the two stroboscopes to a cylindrical lens that generated a sheet of light of 2 mm thickness. The employed optical fiber had two input ends and one common output end. Each input end was connected to each stroboscope and the common output end was connected to the cylindrical lens. The generated light sheet illuminated the x–y plane at the center of the channel span. The lamp input power for each flash was 1.7 J/flash, with a half-width duration ranging from 18 to 23 μs.

Images of the tracers were taken from the direction normal to the light sheet using a monochromatic CCD camera with a resolution of 640×480. A delay generator synchronized the flashes of the stroboscopes to the vertical blank signal of NTSC. Immediately before and after the blank signal, two strobes were flashed. Thus, the two field images with arbitrary small time increment Δt were recorded on each TV frame (Lecordier et al., 1994). The output signal of the CCD camera was directly sent to a personal computer and digitized by an 8-bit frame grabber equipped therein. The spatial resolution corresponding to one pixel was approximately 150 μm. The number of images taken for one experiment was 1000. The measurement was divided into three areas that covered the flow field ranging from $-0.5H$ to $11.5H$ to keep the measurement uncertainty. Each measurement area was approximately 100 mm × 75 mm. The typical time required for image acquisition in a single experiment was about 3 h. The digitized image data were analyzed on a calculation server for further velocity calculation after image acquisition was completed.

3.2. Velocity calculation

Each digitized frame image was first separated into even and odd field images. As each of the separated field images consisted of only every two horizontal lines, the missing lines were reproduced by vertical interpolation so that the field images had the same number of horizontal lines as the general frame image. By comparing the particle-image pattern in a pair of even and odd field images, the velocity vector distributions were computed by the cross-correlation method (Adrian, 1991). The size of the investigation matrix was 19×19 pixels, which roughly corresponded to $0.14H \times 0.14H$.

To obtain higher accuracy in velocity measurement, the displacement of the particle-image patterns between the two field images was calculated at sub-pixel level by applying a three-point estimator with Gaussian peak fitting from the correlation data (Raffel et al., 1998).

4. Experimental conditions

4.1. Uncertainty estimation

Fig. 3 shows the dependence of the mean and the standard deviation of the streamwise velocity on the number of samples used in this experiment. Two typical locations are chosen for evaluation: $\{x/H, y/H\} = \{2.1, 0.0\}$ and $\{3.9, -0.3\}$, where turbulent kinetic energy takes a relatively high value in the shear layer. As seen in Figs. 3(a) and (b), in both positions evaluated, the mean velocity tends to converge within 1.5% deviation relative to that of the 3000-sample case, when the number of samples exceeds 1000. The convergence of the standard deviation shown in Figs. 3(c) and (d) is slower and reaches only 6.2% deviation at 1000 samples. As a compromise between acquisition time and accuracy, the number of samples is therefore set to 1000.

Major source of uncertainty of PIV measurements is considered to be the effect of velocity gradient. Because the uncertainty of the PIV measurement increases with the increasing

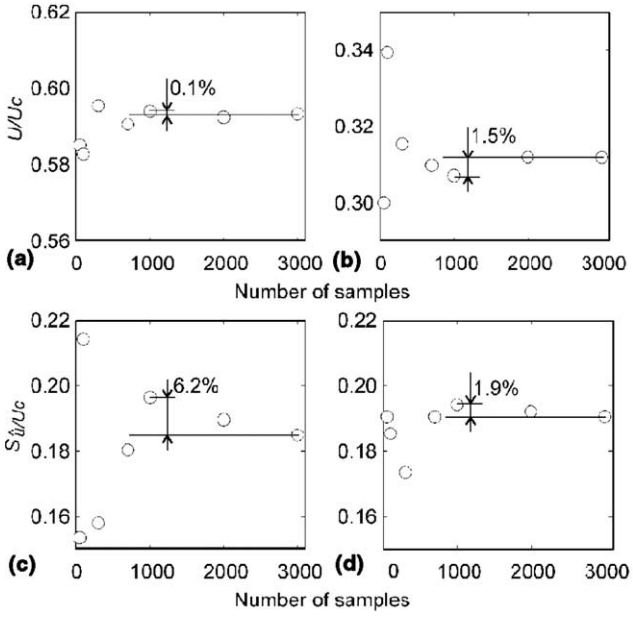

Fig. 3. Influence of the number of samples on the mean streamwise velocity U and the standard deviation S. (a), (c) $x/H = 2.1$, $y/H = 0.0$, (b), (d) $x/H = 3.9$, $y/H = -0.3$.

Table 1
95% coverage of mean and second-order moments of velocity data[a]

Variable	Position $x/H = 3.9$	
	$y/H = 0.5$	$y/H = -0.3$
U	0.010	0.014
V	0.014	0.017
$\overline{uu}$	0.028	0.136
$\overline{vv}$	0.022	0.156
$-\overline{uv}$	0.303	0.134

[a] Values are normalized by the local mean values at the corresponding positions.

local, instantaneous strain rate, the uncertainty evaluation were performed at the locations where the mean velocity gradient was maximum, $\{x/H, y/H\} = \{3.9, -0.3\}$, and moderate, $\{x/H, y/H\} = \{3.9, 0.5\}$, in separated shear layer. Table 1 shows the uncertainty intervals as the 95% coverage of the mean and second-order moments of velocity at these locations. The uncertainty values are normalized by the local mean values at the corresponding positions. The uncertainty of $-\overline{uv}$ at $x/H = 3.9, y/H = 0.5$ is apparently very large because it is normalized by a very small local mean value.

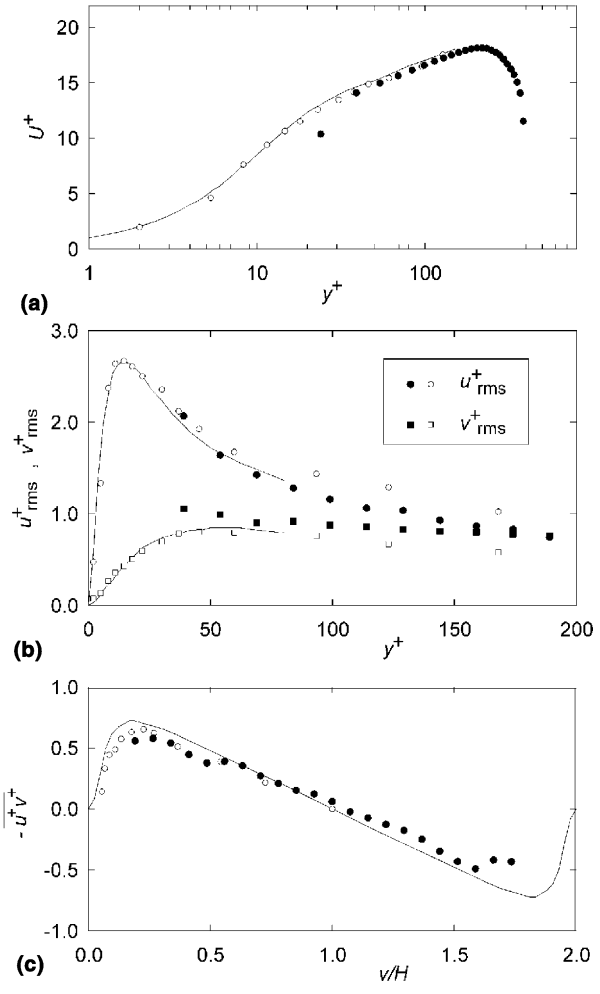

Fig. 4. Profiles of mean velocity and turbulence quantities upstream of the step, $x/H = -0.6$, and those of fully developed turbulent channel flow of Wei and Willmarth (1989) obtained by LDA, $Re = 2970$, and of Kim et al. (1987) obtained by DNS, $Re = 3300$. (a) Mean streamwise velocity, (b) turbulent intensities, (c) Reynolds shear stress: •, ■ present; ○, □, Wei and Willmarth; ——, Kim et al.

4.2. Inlet condition

The profiles of velocity data measured at the inlet, $x/H = -0.6$, are shown in Fig. 4. Reynolds number Re, based on step height H and center velocity of the inlet channel U_c, is 3700. The velocity profiles are compared with the LDA data of Wei and Willmarth (1989) at $Re = 2970$ and the DNS data of Kim et al. (1987) at $Re = 3300$, both for fully developed turbulent channel flows. The mean streamwise velocity profiles are presented in Fig. 4(a). U^+ is the velocity normalized by friction velocity u_τ. y^+ is the distance from the wall normalized by v/u_τ. The friction velocity $u_\tau = 0.010$ m/s is estimated from the empirical skin friction correlation given by Dean (1978). The present data agree with those of the two previous studies of fully developed turbulent channel flow. The ratio $U_c/U_b = 1.16$ is identical to the value for fully developed channel flow proposed by Dean (1978). Fig. 4(b) shows the distributions of turbulent intensity, u^+_{rms} and v^+_{rms}. The present profiles are in accordance with the fully developed flow data, although v^+_{rms} is slightly higher than the reference data. This is due to the difficulty in obtaining sufficient transverse displacement of particle images in the center region of the channel to ensure the accuracy of v there. This problem is avoided in the separated shear layer because it is possible to take a much larger displacement along the y direction in that region. Fig. 4(c) shows Reynolds shear stress $-\overline{u^+v^+}$. The present result lies closely to the linear profile peculiar to the fully developed flow. Although there is a slight influence of the streamwise pressure gradient at this location, this influence is considered to be within the overall ambiguity in velocity measurements. As a whole, it is concluded that the flow at the inlet of the test section is a fully developed turbulent channel flow.

5. Results and discussion

5.1. Time-averaged flow field in unperturbed flow experiment

Prior to the discussion on the effect of perturbation, the flow structure under the unperturbed condition is examined as a baseline for comparison. Fig. 5 shows the velocity vector distribution behind the step at $Re = 3700$. The filled triangular mark on the bottom of the figure denotes the reattachment point, $x_{R_0} = 5.5H$. The flow field shows a recirculating region that includes the clockwise loop of the velocity vectors centered around $x/H = 2.5, y/H = -0.5$. The height of this recirculating region is on the order of the step height. A weak secondary counter clockwise vortex is observed at the corner of the step. Maximum reverse flow is observed at $x/H = 2.9, y/H = -0.9$ and the velocity magnitude there is 18% of U_c. The flow characteristics of the present test case agree with those of other experiments (Chandrsuda and Bradshaw, 1981; Eaton and Johnston, 1981; Driver and

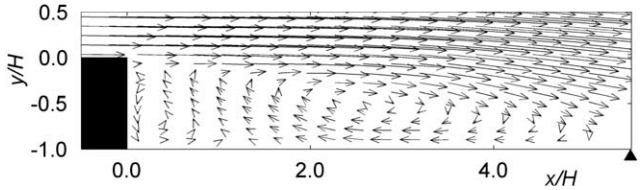

Fig. 5. Velocity vector distribution in the unperturbed flow experiment. Filled triangle indicates the reattachment point, $x/H = 5.5$.

Seegmiller, 1985; Adams and Johnston, 1988; Adachi et al., 1993; Jovic and Driver, 1994).

Time-averaged distributions of streamwise velocity and Reynolds stress at three representative cross-sections: $x/H = 4.0$, in the recirculating region; $x/H = 6.0$, near the reattachment point; and $x/H = 10.0$, further downstream of the reattachment point; are presented in Fig. 6. The results are compared with previous studies. The results of Le et al. (1997) were obtained by DNS at $Re = 5100$ and expansion ratio 1.2. Since their inflow condition was a turbulent boundary layer with non-turbulent free stream, which differed from that of the present study, only the portion $-1.0 < y/H < 0.5$ of their profiles is presented for comparison. Kasagi and Matsunaga (1995) measured the turbulent backward-facing step flow of $Re = 5540$ and expansion ratio 1.5 with 3D-PTV. Although the present experiment underestimated $\overline{u^2}$ in the shear layer at $x/H = 6.0$ and 10.0, the velocity and Reynolds stress profiles of the present study are in fair agreement with those of the two studies. On the whole, it can be said that the present unperturbed flow exhibits the typical characteristics of backward-facing step turbulent flow.

5.2. Variation of reattachment length by the perturbation

The time-averaged reattachment length x_R is shown in Fig. 7 as a function of Strouhal number $St = f_e H/U_c$, with f_e being the perturbation frequency, H the step height and U_c the center velocity of the inlet channel. In the present study, the reattachment point is defined as the point where the time-averaged streamwise velocity nearest to the wall (distance to the wall is about 1.5 mm) changes its direction. The reattachment length shown in Fig. 7 is normalized by that of the unperturbed experiment. The perturbation-frequency characteristic of the reattachment length is almost independent of Re. In all Re cases shown in Fig. 7, the reattachment length first decreases with increasing St before it reaches a minimum near $St = 0.2$, and then increases again. In the present experiment, the reattachment length is reduced by 30% around $St = 0.2$. The results reported by Chun and Sung (1996) and Yoshioka et al. (1998) are compared with the present results in Fig. 7. The results of the present study are consistent with their data but show slightly stronger variation with the change in perturbation frequency. There are some reports on the existence of a dominant frequency in reattaching region of separated turbulent shear layer (Eaton and Johnston, 1980; Silveira Neto et al., 1993; Le et al., 1997). This frequency varies over a certain range, which is shown in Fig. 7. Compared to this, the most effective frequency for the reduction of the reattachment length is around twice as high as the dominant frequency.

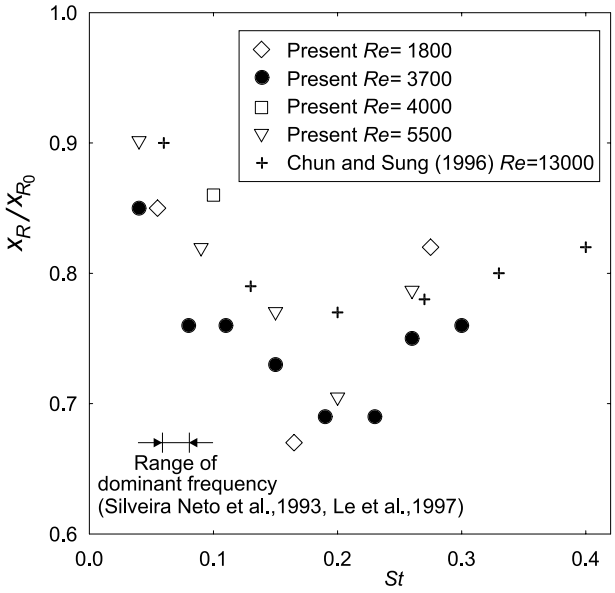

Fig. 7. Reattachment length as a function of St.

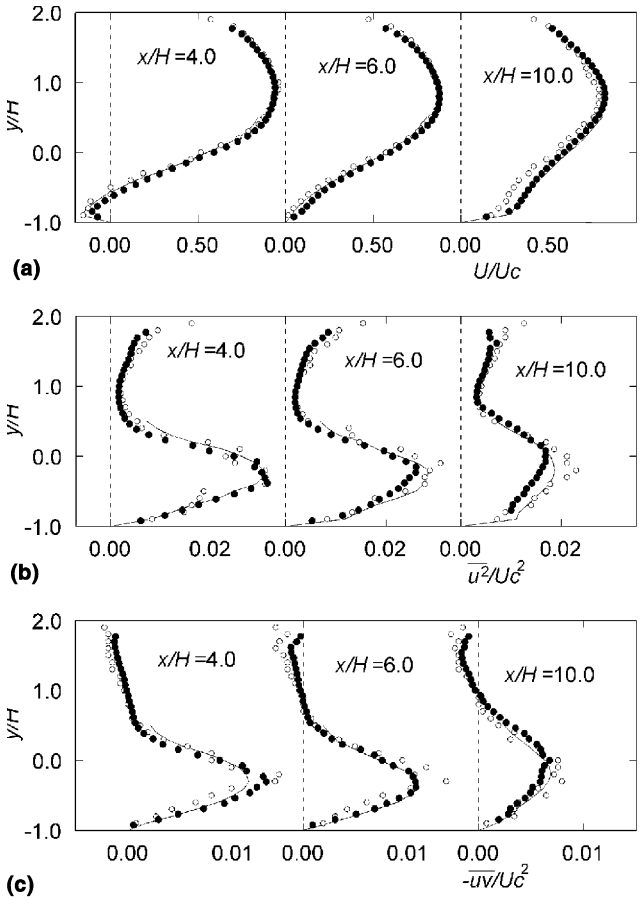

Fig. 6. Comparison of present results, those of Kasagi and Matsunaga (1995) obtained by PTV, $Re = 5540$, and those of Le et al. (1997) obtained by DNS, $Re = 5100$. (a) Mean streamwise velocity, (b) streamwise normal stress, (c) shear stress: •, present; ○, Kasagi and Matsunaga; —— Le et al.

It is considered that reattachment promotion is realized by the additional momentum transfer by the activated turbulent motion achieved by the induced periodic perturbation. In the remaining part of this paper, the time-averaged turbulent statistics will be discussed to evaluate the enhancement of the momentum transfer in the case of $Re = 3700$.

5.3. Effect of perturbation on mean velocity and Reynolds stress

The instantaneous velocity $\hat{u}_i$ may be decomposed into three components:

$$\hat{u}_i = U_i + u_i = U_i + \tilde{u}_i + u_i', \tag{2}$$

where U_i denotes the time averaged-velocity component, while $\tilde{u}_i$ and u_i' denote the fluctuating components whose frequency is equal to and out of f_e, respectively. As the present study discusses the time-averaged flow structure and momentum transport, the time-averaged velocity U_i and the sum of the fluctuating velocity components u_i will be evaluated.

Fig. 8 shows the profiles of the mean streamwise velocity at various streamwise locations. The profiles taken from the velocity measurements with perturbations at three different frequencies are compared with that obtained without perturbation to evaluate the frequency characteristics of the mean flow structure. The three perturbation frequencies selected here are the most effective frequency for reattachment promotion of $St = 0.19$, and the surrounding two frequencies of $St = 0.08$ and $St = 0.30$. These frequencies will be called the "optimum", "lower" and "higher" frequencies hereafter. The reattachment lengths in these three experiments are $3.8H$, $4.2H$ and $4.2H$, respectively.

There is almost no difference among the profiles of the four experiments conducted in the region immediately behind the step, $x/H = 2.0$. In the somewhat downstream region, $x/H = 4.0$, a marked difference among the profiles is observed near the wall. No reverse flow is observed in the experiment with the optimum-frequency perturbation, while the other experiments show a reverse flow near the bottom wall. The highest reverse flow rate is observed in the unperturbed flow experiment. Boundary-layer redevelopment behind the reattachment point is suppressed in perturbed flow experiments although the flow reattaches earlier than that in the unperturbed flow experiment. This finding indicates that the vortical structures generated upstream still exist in this region. In the experiment with lower-frequency perturbation, remarkable flow acceleration is observed in the center region of the shear layer (around $y/H = -0.3$) downstream of the reattachment region, $x/H \geqslant 6$. In contrast, in the optimum-frequency perturbation experiment, flow acceleration was observed in the outer region of the redeveloping wall boundary layer downstream of the reattachment region, $x/H \geqslant 6$. On the other hand, the higher-frequency perturbation seems to have a weaker effect on the entire region of the shear layer. It is concluded that periodic perturbation accelerates flow in the shear layer but its effect depends on the frequency of the applied perturbation.

The difference in the mean-velocity profile in the shear layer reflects the difference in the momentum transfer across the channel. To clarify this, distributions of the Reynolds stress components are investigated next. Figs. 9(a) and (b) show the distributions of normal components $\overline{u^2}$ and $\overline{v^2}$, respectively.

Unlike the case of the mean streamwise velocity, the effect of perturbation is found in the shear layer even in the region immediately behind the step. As shown in Fig. 9(a), at $x/H = 2.0$, the values of $\overline{u^2}$ in all perturbed flow experiments are increased in the separated shear layer compared to that in the unperturbed flow experiment. Somewhat downstream, at $x/H = 4.0$, $\overline{u^2}$ of the optimum-frequency experiment is increased in the shear layer and takes the highest peak in the central region of the shear layer. In contrast, in the lower-frequency perturbation experiment, the peak of $\overline{u^2}$ is observed closer to the bottom wall. It should be noted that this lower-frequency perturbation also increases $\overline{u^2}$ in the upper region of $y/H \geqslant 0.5$ at $x/H = 4.0$. Even in downstream region, $x/H \geqslant 6.0$, the $\overline{u^2}$ values in all perturbed flow experiments are larger than that in the unperturbed flow experiment. Particularly in the lower-frequency perturbation experiment, $\overline{u^2}$ has a higher value in the region downstream of the reattachment zone, $x/H \geqslant 6.0$, than those of the other experiments.

The profiles of $\overline{v^2}$ presented in Fig. 9(b) show a trend similar to that of $\overline{u^2}$. In the experiment with the optimum-frequency perturbation, $\overline{v^2}$ increases in the shear layer at $2 \leqslant x/H \leqslant 4$ and then decays downstream. In the experiment with the lower-frequency perturbation, although $\overline{v^2}$ remains lower than those in the other perturbed flow experiments at $x/H = 2.0$, it gradually increases downstream and then takes the largest value at downstream region, $x/H \geqslant 6.0$. In the experiment with the higher-frequency perturbation, $\overline{v^2}$ shows a slight increase compared to that in the unperturbed flow experiment in the shear layer at $x/H = 2.0$, and keeps decreasing at downstream locations.

Fig. 9(c) shows the Reynolds shear stress $-\overline{uv}$. The perturbations at all three frequencies increased $-\overline{uv}$ in all measured sections. The effect of perturbation is more remarkable for the two normal stress components than for this shear stress component. It is probable that the increase in normal stress is partly due to the variation of the mass flow rate as perturbation is applied. On the other hand, the increase in this shear stress component indicates the enhancement of vortical motion produced by perturbation. Both optimum- and lower-frequency perturbations increase $-\overline{uv}$ in the shear layer near the reattachment point, $x/H = 4.0$. The lower-frequency perturbation increases $-\overline{uv}$ not only in the reattached shear layer but also in the entire area of the measured section at downstream region, $x/H \geqslant 6.0$. This suggests that organized vortical structures induced by the lower-frequency perturbation are indeed distributed in this region. On the other hand, compared to the unperturbed flow experiment, almost no remarkable increase in $-\overline{uv}$ is observed in the experiment with the higher-frequency perturbation though a slight increase is observed in the shear layer immediately behind the step, $x/H = 2.0$. It is concluded that the optimum-frequency perturbation increases Reynolds stress near the reattachment region and the lower-frequency perturbation increases in the region downstream of the reattachment zone. The higher-frequency perturbation has weaker effect than the other two frequency perturbations.

As reattachment promotion is attributable to the turbulent motion activated by perturbation, the effect of perturbation on the energy transfer from the mean flow to the turbulent motion is evaluated. This energy transfer is indicated by the production rate of Reynolds stress. The production term in the transport equation of time-averaged Reynolds stress is expressed as:

$$P_{ij} = -\overline{u_i u_k}\frac{\partial U_j}{\partial x_k} - \overline{u_j u_k}\frac{\partial U_i}{\partial x_k}. \tag{3}$$

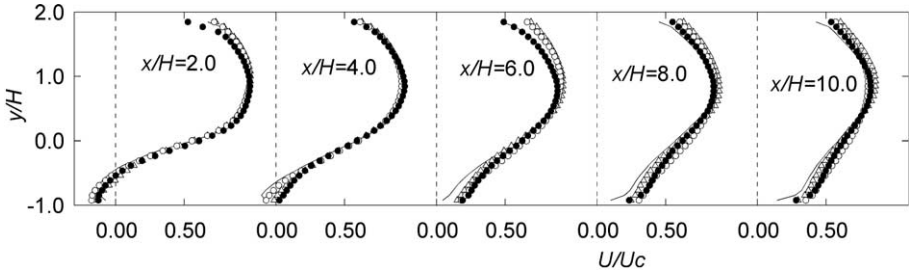

Fig. 8. Mean streamwise velocity profiles at various streamwise locations: ——, unperturbed; ○, $St = 0.08$; •, $St = 0.19$; △, $St = 0.30$.

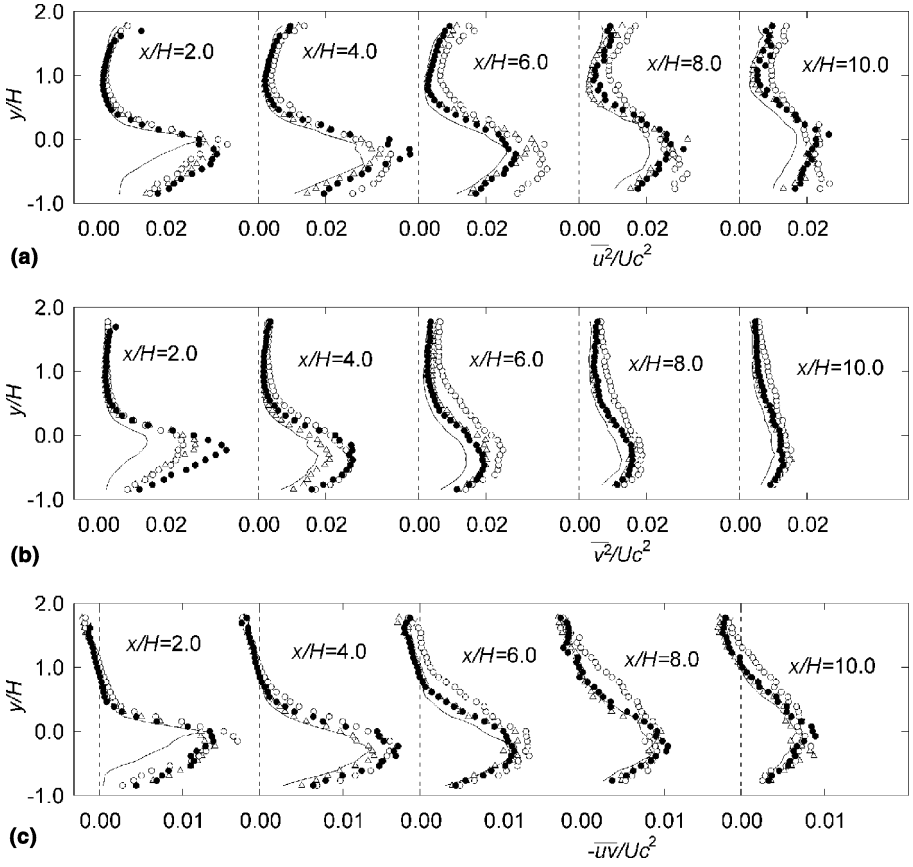

Fig. 9. Reynolds stress profiles at various streamwise locations. (a) Streamwise normal stress, (b) transverse normal stress, (c) shear stress. Symbols as in Fig. 8.

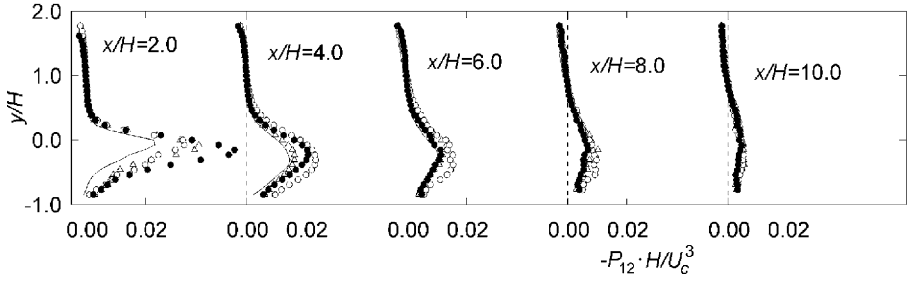

Fig. 10. Production rate of Reynolds shear stress $-P_{12}\cdot H/U_c^3$ at various streamwise locations. Symbols as in Fig. 8.

Fig. 10 shows the distribution of $-P_{12}$. Only the shear stress component is presented here, since this component has a dominant effect in terms of the momentum transport across the mean shear. The increase in production rate due to the applied perturbation is limited in the separated shear layer, as shown in Fig. 10. In the optimum-frequency case, the profile of the production rate shows a peak in the shear layer immediately behind the step, $x/H = 2.0$. This peak gradually disappears downstream and then, at $x/H > 6.0$, the profile shows almost the same shape as that of the unperturbed case. In the lower-frequency case, although the profile shows a lower peak at $x/H = 2.0$ than those of the other two frequency cases, the profile keeps the highest among the four cases tested in downstream region, $x/H > 4.0$. On the other hand, in the higher-frequency case, although the peak value of the production rate is next to that of the optimum-frequency case at $x/H = 2.0$, it shows a rapid decay downstream of this region. As a whole, the perturbation-frequency characteristics of the production-rate distribution, the energy transfer from mean flow to turbulent motion, are similar to that of Reynolds stress itself. The effect of perturbation on reattachment promotion is supported by the increase in the effect of energy transfer.

5.4. Perturbation frequency characteristics of momentum transfer effect

The increase in the production rate of Reynolds stress due to the applied periodic perturbation is attributable to the organized vortex motion in the separated shear layer. Detailed discussion on the organized vortical motion based on the phase-averaged flow field is presented in Yoshioka et al. (2001).

The question is why the optimum frequency exists. The answer to the question may be indicated by the evolution of Reynolds stress along the shear layer. At the optimum-frequency, the remarkable increase in Reynolds stress is found at $x/H = 2.0$ and 4.0, as seen in Fig. 9. The lower-frequency perturbation increases Reynolds stress further downstream compared to the optimum-frequency perturbation because the scale of vortical structures that this lower-frequency perturbation induced are larger than those of the optimum-frequency. This lower-frequency perturbation has less effect on reattachment promotion because the influence of the large scale vortex motion appears after the flow reattaches. On the other hand, when the frequency is higher than the optimum range, the vortices generated by perturbation decay faster without influence the shear layer. The similar tendency is presented in an experiment in a plane asymmetric diffuser (Obi et al., 1997). While it is considered that the perturbation with too high frequency decay too fast, that with too low frequency provides only weak effect before the flow reattachment. The optimum-frequency range is realized as a consequence of these two different reasons.

6. Concluding remarks

The turbulence statistics of a periodically perturbed flow over a backward-facing step is experimentally investigated using PIV and the effect of applied perturbation on flow reattachment is evaluated. The reattachment length varies with the applied perturbation frequency, being shortened by 30% at the optimum frequency, $St = 0.19$. Corresponding to this promotion of reattachment, Reynolds stress is increased in the shear layer.

The effect of perturbation on the increase in Reynolds stress depends on its frequency. The location where Reynolds stress is increased from that in the unperturbed flow experiment varies with the applied perturbation frequency. The optimum-frequency perturbation increases Reynolds stress near the reattachment region. The lower-frequency perturbation increases Reynolds stress more than the optimum-frequency perturbation, though the increase is observed downstream of the reattachment region. The region where the higher-frequency perturbation increases Reynolds stress is limited to the early stage of the recirculating region.

The increased Reynolds stress enhances the momentum transfer in the separated shear layer, enabling the promotion of reattachment. In the experiment with the optimum-frequency perturbation, the shortest reattachment length is obtained as the momentum transfer is enhanced in the reattachment region, compared with the other two frequency experiments.

Acknowledgements

Part of the present study is supported by Ministry of Education though Grand-in-Aid for Scientific Research. The authors are grateful to Professor K. Nishino of Yokohama National University, Professor K. Hishida and his coworkers at Keio University for their valuable advice on PIV measurement, and EBARA Research Co., Ltd. for facilitating the pump system. Mr. N. Fuse of Keio University is also acknowledged for preparation of the instruments and assistance in the experiment.

References

Adachi, T., Nishino, K., Torii, K., 1993. Digital PTV measurement of a separated air flow behind a backward-facing step. Journal of Flow Visualization and Image Processing 1, 317–335.

Adams, E.W., Johnston, J.P., 1988. Effects of the separating shear layer on the reattachment flow structure Part 2: Reattachment length and wall shear stress. Experiments in Fluids 6, 493–499.

Adrian, R.J., 1991. Particle-imaging technique for experimental fluid mechanics. Annual Review of Fluid Mechanics 23, 261–394.

Bhattacharjee, S., Scheelke, B., Troutt, T.R., 1986. Modification of vortex interactions in a reattaching separated flow. AIAA Journal 24, 623–629.

Chandrsuda, C., Bradshaw, P., 1981. Turbulence structure of a reattaching mixing layer. Journal of Fluid Mechanics 110, 171–194.

Chun, K.B., Sung, H.J., 1996. Control of turbulent separated flow over a backward-facing step by local forcing. Experiments in Fluids 21, 417–426.

Chun, K.B., Sung, H.J., 1998. Visualization of a locally forced separated flow over a backward-facing step. Experiments in Fluids 25, 133–142.

Dean, R.B., 1978. Reynolds number dependence of skin friction and other bulk flow variables in two-dimensional rectangular duct flow. Transactions of the ASME Journal of Fluids Engineering 100, 215–223.

Driver, D.M., Seegmiller, H.L., 1985. Features of a reattaching turbulent shear layer in divergent channel flow. AIAA Journal 23, 163–171.

Eaton, J.K., Johnston, J.P., 1980. Turbulent flow reattachment: an experimental study of the flow and structure behind a backward-facing step. Report MD-39, Thermosciences Division, Department of Mechanical Engineering, Stanford University.

Eaton, J.K., Johnston, J.P., 1981. A review of research on subsonic turbulent flow reattachment. AIAA Journal 19, 1093–1100.

Jovic, S., Driver, D.M., 1994. Backward-facing step measurements at low Reynolds number, $Re_h = 5000$. NASA Technical Memorandum, 108807.

Kasagi, N., Matsunaga, A., 1995. Three-dimensional particle-tracking velocimetry measurement of turbulence statistics and energy budget in a backward-facing step flow. International Journal of Heat and Fluid Flow 16, 477–485.

Kim, J., Moin, P., Moser, R., 1987. Turbulence statistics in fully developed channel flow at low Reynolds number. Journal of Fluid Mechanics 177, 133–166.

Kiya, M., Shimizu, M., Mochizuki, O., 1997. Sinusoidal forcing of a turbulent separation bubble. Journal of Fluid Mechanics 342, 119–139.

Le, H., Moin, P., Kim, J., 1997. Direct numerical simulation of turbulent flow over a backward-facing step. Journal of Fluid Mechanics 330, 349–374.

Lecordier, B., Mouqallid, M., Vottier, S., Rouland, E., Allano, D., Trinite, M., 1994. CCD recording method for cross-correlation PIV development in unstationary high speed flow. Experiments in Fluids 17, 205–208.

Masuda, S., Obi, S., Aoki, K., 1994. Control of turbulent separating and reattaching flow by periodic perturbations. Turbulence Control, ASME, FED-Vol. 193, pp. 55–61.

Nishri, B., Wygnanski, I., 1998. Effects of periodic excitation on turbulent flow separation from a flap. AIAA Journal 36, 547–556.

Obi, S., Ishibashi, N., Masuda, S., 1997. The mechanism of momentum transfer enhancement in the periodically perturbed turbulent separated flow. In: Hanjalić, K., Peeters, T.W.J. (Eds.), Turbulence, Heat and Mass Transfer 2. Delft University Press, Delft, pp. 835–844.

Raffel, M., Willert, C.E., Kompenhans, J., 1998. Particle Image Velocimetry: a practical guide. Springer, Berlin.

Seifert, A., Pack, L.G., 1999. Oscillatory control of separation at high Reynolds numbers. AIAA Journal 37, 1062–1071.

Sigurdson, L.W., 1995. The structure and control of a turbulent reattaching flow. Journal of Fluid Mechanics 298, 139–165.

Silveira Neto, A., Grand, D., Metais, O., Lesieur, M., 1993. A numerical investigation of the coherent vortices in turbulence behind a backward-facing step. Journal of Fluid Mechanics 256, 1–25.

Wei, T., Willmarth, W.W., 1989. Reynolds-number effects on the structure of a turbulent channel flow. Journal of Fluid Mechanics 204, 57–95.

Yoshioka, S., Obi, S., Masuda, S., 1998. Role of the vortex motion in the periodically perturbed turbulent flow over the backward-facing step. Proceedings of the fourth KSME-JSME Fluids Engineering Conference, 585–588.

Yoshioka, S., Obi, S., Masuda, S., 2001. Organized vortex motion in periodically perturbed turbulent separated flow over a backward-facing step. International Journal of Heat and Fluid Flow, 22, 301–307.